Journal of Power Sources 196 (2011) 7555–7563

Contents lists available at ScienceDirect

Journal of Power Sources

journal homepage: www.elsevier.com/locate/jpowsour

The impact of flow distributors on the performance of solid oxide fuel cell—Part II: Electrochemical impedance measurements

S.S. Shy[a,b,*], C.M. Huang[a], H.H. Li[a], C.H. Lee[c]

[a] Department of Mechanical Engineering, National Central University, Jhong-li 32001, Taiwan
[b] Center for Energy Research, College of Engineering, National Central University, Taiwan
[c] Institute of Nuclear Energy Research, Lung-tan, Tao-yuan 32546, Taiwan

ARTICLE INFO

Article history:
Received 15 February 2011
Received in revised form 7 April 2011
Accepted 8 April 2011
Available online 22 April 2011

Keywords:
Planar anode-supported solid oxide fuel cell
Flow distributors
Electrochemical impedance spectroscopy
Anodic re-oxidation
Anodic microstructures

ABSTRACT

This paper presents newly measured electrochemical impedance spectra of two sets of nearly identical single-cell stacks except using different designs of flow distributors for planar solid oxide fuel cells (SOFCs). It is found that by using small guide vanes around the feed header of commonly used rib-channel flow distributors to improve significantly the degree of flow uniformity, values of ohmic and polarization resistances of the single-cell stack can be decreased by 32% and 60% as compared to that without using guide vanes under the same experimental conditions at 0.6 V and 850 °C. This finding explains why by improving flow uniformity in interconnects can result in more than 10% increase of the cell power density. Moreover, the higher resistances measured for the case without using guide vanes are attributed to the anodic re-oxidation behavior due to non-uniform flow distributions in interconnects, as also verified by SEM images of anodic microstructures. These results show that the improvement of flow uniformity in flow distributors is useful to increase the performance and the longevity of planar SOFCs.

1. Introduction

This is the third paper emanating from a series of numerical and experimental studies [1,2] aiming to address the impact of flow distributors on the cell performance of planar solid oxide fuel cell (SOFC). In it we report for the first time the newly measured electrochemical impedance spectra and anodic re-oxidation microstructures of two sets of nearly identical single-cell stacks having flow distributors in both anode and cathode under the same operating conditions except that different designs of flow distributors are applied in these two single-cell stacks. Hence, the obtained results can be used to explain why by improving flow uniformity in interconnects not only can result in more than 10% increase of the cell power density but also can avoid the cell degradation caused by the anodic re-oxidation.

In our previous numerical and experimental studies [1,2], we used the term "single-cell stack", same as other research groups such as Yakabe et al. [3,4], to distinguish from "single cell" that only consisted of a positive electrode–electrolyte–negative electrode (PEN) and current collectors without flow distributors. The first paper dealt with the issue of "*what*", in which four different designs of commonly used rib-channel flow distributors having different degrees of flow uniformity were proposed [1]. It should be noted that the flow uniformity has been verified by measuring flow velocities and thus flow rates in each of twelve rib-channels, as can be found from Figs. 6 and 7 of Ref. [1]. These four different flow distributors were then used in several 3D electrochemical numerical models to predict the influence of flow uniformity in interconnects on the cell performance of planar SOFC [1]. It was found that a new design, using simple small guide vanes equally spaced around the feed header of the double-inlet/single-outlet rib-channel flow distributor, can significantly improve the degree of flow uniformity in interconnects, resulting in an increase of the peak power density (PPD) of single-cell stacks up to 11% [1]. In order to validate the numerical finding [1] and show "*how*" exactly the cell performance of single-cell stacks would vary with a change in the degree of flow uniformity, a real SOFC test rig was established, as presented in our second paper [2]. In [2], the power generating characteristics of two sets of nearly identical Ni–YSZ anode-supported single-cell stacks under exactly the same experimental conditions, except using or not using small guide vanes around the feed header of rib-channel flow distributors, were measured and compared. Hence, the numerical result indicating that by improving flow uniformity in interconnects can result in more than 10% increase of the cell power density was then experimentally validated. Using the same methodology as in [2] and further applying the electrochemical impedance spectroscopy (EIS) as well as the SEM microstructure visualization, the present study measures the

* Corresponding author at: Department of Mechanical Engineering, National Central University, 300 Jhong-da Road, Jhong-li, Tao-yuan 32001, Taiwan.
Tel.: +886 3 426 7327; fax: +886 3 427 6157.
E-mail address: sshy@ncu.edu.tw (S.S. Shy).

0378-7753/$ – see front matter © 2011 Elsevier B.V. All rights reserved.
doi:10.1016/j.jpowsour.2011.04.021

impedance spectra and the anodic re-oxidation microstructures for the aforementioned two sets of nearly identical single-cell stacks using different flow distributors. Thus, the final "*why*" issue concerning the impact of flow distributors on the performance and the anodic degradation of planar SOFC can be addressed.

The EIS technology, also known as the AC impedance technology, is a very useful tool for the investigation of the corrosions of materials, the performance of electrochemical devices, and the degradation mechanisms in SOFCs, see for instances Refs. [5–14] among many others. Because almost all kinds of transport phenomena in any given electrochemical devices including those in SOFCs have their own inherent electrochemical rates, the complex diffusion processes and electrochemical degradation mechanisms in SOFCs can be thus diagnosed by the EIS technology. For a typical impedance measurement of any electrochemical devices, a small perturbed voltage signal, $V(t) = V_0 \cos(\omega t + \varphi)$, is commonly applied onto the device to obtain a current response, $I(t) = I_0 \cos(\omega t + \psi)$, where V_0 and I_0 are the amplitudes of the voltage signal and the current response, ω is the angular frequency ($\omega = 2\pi f$), and φ and ψ are the initial phase angles of the voltage signal and the current response. Similar to the Ohm's law, the expression of the voltage signal and the current response can be converted from a time domain to a complex frequency domain via the Fourier transformation. Thus, the impedance function $Z(i\omega) = V(i\omega)/I(i\omega)$, where the imaginary number i; $(-1)^{0.5}$; $\exp(i\pi/2)$ indicating an anticlockwise rotation of the impedance vector by $\pi/2$ relative to the x-axis. In the complex plane, the real part of the impedance function is denoted as Re(Z); $Z' = |Z|\cos(\theta)$ and the imaginary part $\mathrm{Im}(Z) \equiv Z'' = |Z|\sin(\theta)$, where the phase difference $\theta = \varphi - \psi = \tan^{-1}(Z''/Z')$ and $|Z| = [(Z')^2 + (Z'')^2]^{1/2}$. Therefore, the plot of $-\mathrm{Im}(Z)$ against Re(Z) is the well-known Nyquist plot providing the information on the ohmic and polarization resistances, R_Ω and R_P, of the measured electrochemical device for electrochemical performance analyses [5–11]. However, the important frequencies associated with specific data points on these impedance spectra curves cannot be directly found from the Nyquist plot, but they can be obtained from the Bode plot indicating the impedance and the phase-shift as a function of the frequency [11]. In this study, both the Nyquist and the Bode plots for the aforementioned two sets of single-cell stacks using different flow distributors are measured and compared in order to explain the final "*why*" issue concerning the impact of flow distributors on the cell performance and the anodic degradation of planar SOFC. For a detail treatment on key concepts of EIS models and measurements, the reader is directed to Refs. [11,12].

Concerning the anodic degradation of planar SOFC, Gong et al. [13] categorized the sulfur-tolerant anode materials for the application of SOFC and highlighted possible combined designs of available materials in order to achieve a balance between stability and performance of the anode materials. Also, Iwanschitz et al. [14] investigated the anodic degradation of SOFC upon reduction and oxidation (redox) cycling, one of the major degradation mechanisms in SOFC, and they reported a decrease of the length of the triple-phase boundary due to the changes of the anodic microstructures during the operation of SOFC that can block the mass diffusion pathway of supplied gases. Furthermore, Liu et al. [15] investigated the re-oxidation and reduction of a NiO–YSZ/YSZ/LSM–YSZ anode-supported button cell by monitoring variations of the ohmic resistance under the open-circuit voltage (OCV) condition. They found that values of R_Ω increase with the anodic re-oxidation, because the Ni re-oxidation to NiO can increase the resistance of the electron transfer in anode. Similarly, Laurencin et al. [16] investigated damage mechanisms of the Ni–YSZ cermet re-oxidation in an anode-supported cell using a direct air oxidation (i.e., fuel shutdown) or using an ionic current (i.e., fuel starvation). In the latter case using fuel starvation, a thin layer of the cermet was electrochemically re-oxidized at 800 °C and then reduced under a hydrogen stream, by which such a redox cycle was repeated until the occurrence of serious cell degradation [16]. These EIS data obtained under the OCV condition showed that values of R_Ω increased significantly with increasing redox cycles, while values of the polarization resistance only increased slightly [16]. These previous results suggested that under the OCV condition only values of R_Ω were sensitive to the effect of redox. Though much has been learned on the redox of anode-supported button cells without interconnects under the OCV condition using EIS models and measurements [14–16], still little is known concerning variations of R_Ω and R_P for even a single-cell stack with interconnects under loaded conditions. Therefore, the key objective of this study is to measure and compare variations of R_Ω and R_P with the cell voltages under both unloaded and loaded conditions for the aforementioned two sets of nearly identical single-cell stacks except using different flow distributors via the EIS diagnosis.

The following section describes experimental methods and arrangements used in the study, including (1) a brief description of the test rig and the arrangement of anode and cathode connecting wires to the EIS measuring device, (2) measurements of electrochemical impedance spectra, and (3) measurements of SEM microstructure images for both anode and cathode surfaces of the PEN after 100 h of operation. Both impedance spectra data and SEM microstructures are then used to address effects of flow uniformity in interconnects on the performance and the anodic degradation of the single-cell stacks. We shall show that the re-oxidation behaviors in anode observed only in the case without using guide vanes are due to non-uniform flow distributions in interconnects. Finally, an equivalence circuit model is proposed in attempt to interpret these impedance data.

2. Experimental methods

2.1. Single-cell stack test using two different flow distributors

A SOFC testing platform was recently developed to measure the power-generating characteristics of the single-cell stack having flow distributors in both anode and cathode, as described in [2]. For completeness, a brief description of the test rig is given together with new modifications for EIS measurements. The left part of Fig. 1 presents a photograph showing the arrangement of the testing single-cell stack which is embedded in a ceramic housing inside a temperature-controlled furnace, whereas the middle part of Fig. 1 is an exploding sketch of such single-cell stack along with anodic and cathodic connecting wires to the EIS measuring devices on the right part of Fig. 1. The vertical tubular furnace (Fig. 1) can be used to heat up the single-cell stack from the room temperature to an operating temperature up to 1000 °C. In this study, the single-cell stack test is performed at a fixed temperature of $T = 850$ °C. Same as our previous study [2], we use the commercial anode-supported PEN (ASC 3 purchased from H.C. Starck) to perform the present power and impedance measurements. The structure and compositions of the PEN (ASC 3) are consisted of an anode support layer of NiO–YSZ (Yttria-stabilized Zirconia; Y_2O_2 doped with ZrO_2), an anode functional layer of NiO–YSZ, the electrolyte of YSZ, and a cathode functional layer of YSZ–LSM/LSM (Lanthanum Strontium Manganese oxide, $La_{0.65}Sr_{0.3}Mn_{1.0}O_3$; double layer). Therefore, the single cell is assembled by the aforementioned commercial anode-supported PEN (ASC 3) with a reactive area of 40 mm × 40 mm which is 16 times larger than that of commonly used button cells, a crofer 22-APU supporting frame, and two current collectors using a porous nickel sponge on the anode side and a platinum mesh on the cathode side for the collection of the electrode current. Then the PEN, the metallic frame, and the current collectors are sand-

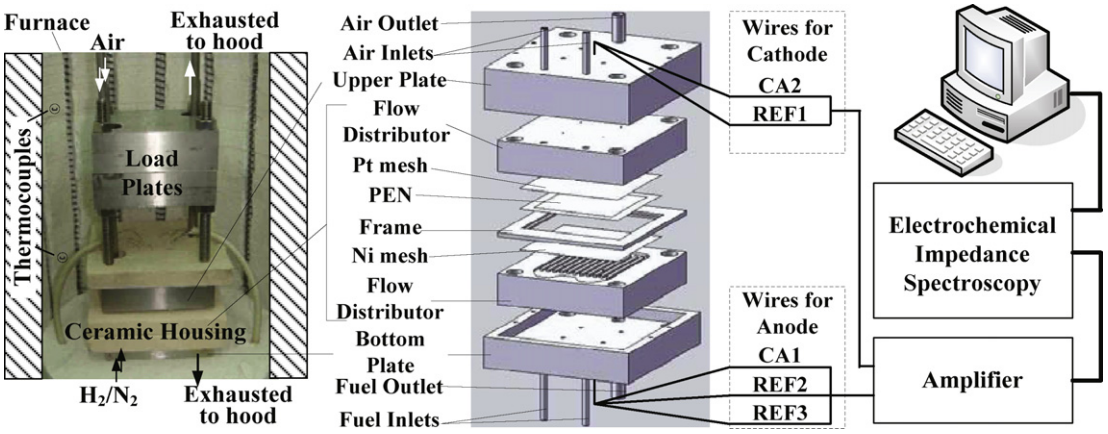

Fig. 1. Photograph of the test rig inside a furnace (left) and the exploding sketch of a single-cell stack using rib-channel flow distributors (middle) in both anode and cathode along with connecting wires to the EIS measuring devices (right).

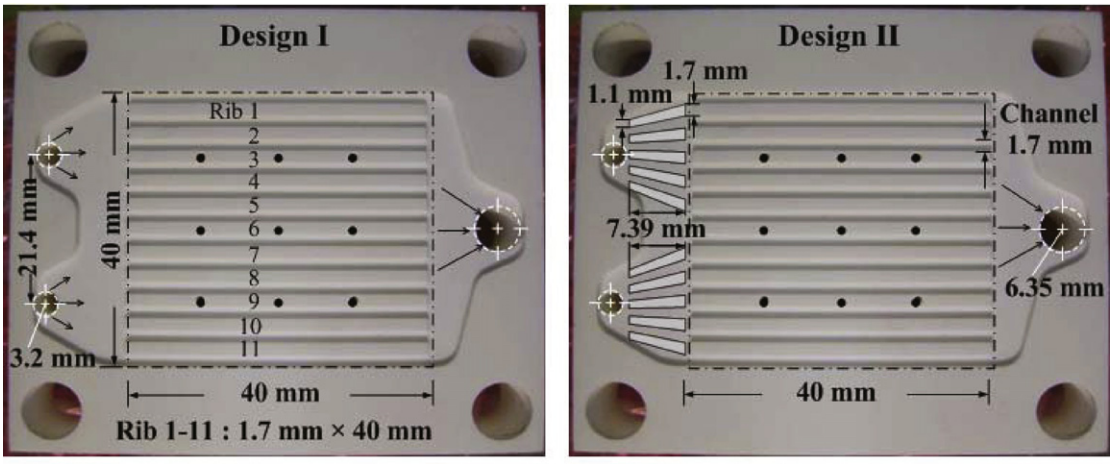

(a) Two different flow distributors

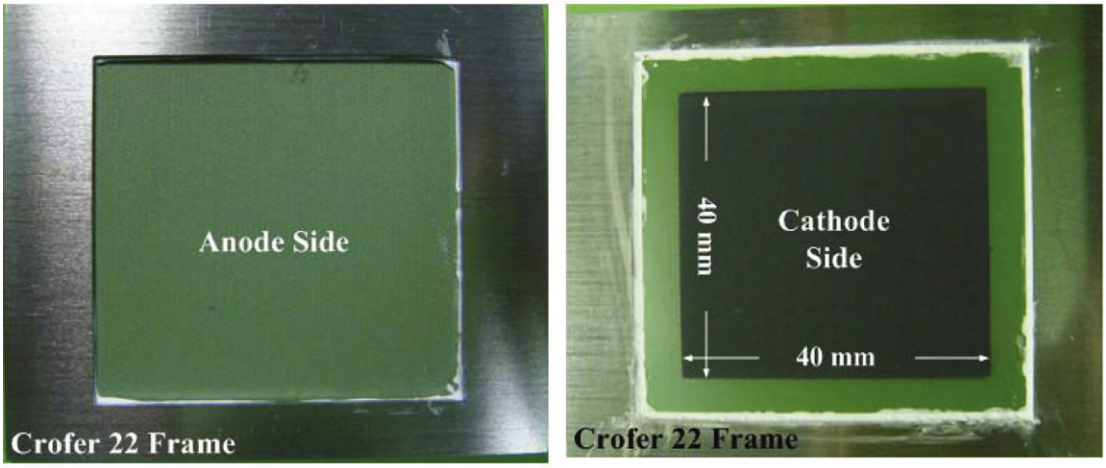

(b) PEN and frame

Fig. 2. (a) Two flow distributors, designs I and II, having the same double-inlet/single-outlet rib-channels, but only the design II using 10 small guide vanes equally positioned around the feed header, where precise dimensions of 11 equal-size ribs, 12 equal-size channels, feed header, and guide vanes are also indicated. Each of 12 channels and/or 11 ribs has 0.7 mm width and 40 mm long. (b) Photographs showing both anode and cathode sides of the PEN with crofer 22 frames before operation, where the white square strips on the cathode side are ceramic sealants to prevent any possible gas leakage at the frame.

wiched by the upper and lower flow distributors (please see both Figs. 1 and 2a) to form a single-cell stack. Note that the use of the metallic frame is to provide the mechanical support to the PEN and further prevent the possible cross-leakages between fuel and oxidant from both feed and exhaust headers of flow distributors. Both flow distributors, designs I and II as indicated in Fig. 2a without and with guide vanes, have nine small holes on their rib-channel area allowing the access of the voltage and current probes for measurements. For the sake of safety, several flame arresters are used and installed along the hydrogen supplied lines and cylinders. Also, the hydrogen gas detectors with the alarm system are also applied near the furnace to monitor possible hydrogen leakages. During the test, the exit gases from the single-cell stack are exhausted by a specially designed hood to the atmosphere after diluting with additional air.

In order to avoid the poisoning problem of the electrodes due to the chromium (Cr) volatilization from the metallic flow distributors at high-temperature conditions [17], we fabricate both anodic and cathodic flow distributors using aluminum oxide materials. As shown in Fig. 2a, two different flow distributors, designs I and II, are used in this study. Both designs have the same double-inlet/single-outlet rib-channels, but only the design II applies 10 small guide vanes equally positioned around the feed header (Fig. 2a) which can effectively improve the flow uniformity in flow distributors to be much better than that of design I. Same as [2], this study also applies 3-kg loading plates (see the left part of Fig. 1) to achieve a good electrical contact among the PEN and the two current collectors. In addition, the present single-cell stack is not tightly screwed having a seal-less assembly, so that the coefficient of thermal expansion (CTE) matching problem among different components of the single-cell stack can be eliminated [18]. It should be noted that by applying such seal-less assembly, one should avoid the cross-leakages of fuel and air in the single-cell stack that can result in serious cell degradation. Hence, two important things must be arranged. First, ceramic sealants must be carefully applied on the crofer 22-APU supporting frame for both anode and cathode sides to prevent any possible gas leakage at the frame, as can be clearly seen from Fig. 2b where the white square strips are ceramic sealants. Secondly, the flow rate of the anode must be kept equal to or slightly higher than that of the cathode in order to make sure no air leakage to the anode. In the present study, the flow rates of both anode and cathode sides for all experiments are kept the same ($Q_{H_2} = Q_{AIR} = 1$ slpm). Since both the mismatch of CTE among components and the Cr-poisoning problems can lead to rapid cell degradation [19], the above arrangements are essential to circumvent these complex problems. Thus, a clear-cut result concerning the impact of flow distributors on the performance and the anodic degradation of single-cell stacks can be obtained.

2.2. Testing procedures and impedance measurements

Since the standardization of the testing procedure is essential in order to obtain repeatable and reliable experimental data [20,21], we apply the same testing procedure proposed by Haanappel and Smith [20] for the present cell performance and impedance spectra measurements. A high reduction temperature at $T = 850\,^{\circ}C$ during the 24-h anode reduction process to achieve a higher cell performance is also applied in the present study. These measurements can be divided by three time stages. The first stage is the 24-h anode reduction period starting when $T = 850\,^{\circ}C$, where the flow rates in anode and cathode are, respectively, $Q_{anode} = 280\,cm^3\,min^{-1}$ ($80\,cm^3\,min^{-1}$ of $H_2 + 200\,cm^3\,min^{-1}$ of N_2) and $Q_{cathode} = 80\,cm^3\,min^{-1}$ of Air. After the completion of the anode reduction, Q_{anode} and $Q_{cathode}$ are very slowly modulated to the designed flow rates of $Q_{anode} = Q_{cathode} = 1000\,cm^3\,min^{-1}$, with an increment of no more than $100\,cm^3\,min^{-1}$, anode first and cathode, and then waiting for 30 min before the next increment to avoid any possible cell damage from a too-large-variation of flow rates and thus cell temperature. This process takes about 6 h, because the anode has 12 increments including 9 times of $100\,cm^3\,min^{-1}$ increment, 1 time of $20\,cm^3\,min^{-1}$ increment and the final 2 times of $100\,cm^3\,min^{-1}$ N_2 decrement, while the cathode has 10 times increments (9 times of $100\,cm^3\,min^{-1}$ increment plus 1 time of $20\,cm^3\,min^{-1}$ increment). The second is the data taking period, where the flow rate in anode is always kept equal to that of the cathode. This data taking process takes about 1 h starting from the OCV condition to various loaded conditions, with an increment of 0.2 A ($0.0125\,A\,cm^{-2}$). Each data point takes about 1 min to measure via the time average procedure. Finally, the third stage is to let the cell operate at a fixed voltage of 0.7 V for 100 h operation. For detailed descriptions on the start-up procedure, the reader is directed to [2].

The impedance spectra of two sets of nearly identical single-cell stacks are measured by the AC impedance analyzer (Bio-Logic, model SP-150) together with a current amplifier (Biologic, VMP3) to extend the measuring range of the operating current from ±800 mA to ±10 A. However, it is rather difficult to employ a reference electrode on the present square-shape large PEN, so that we apply the two-electrode system for EIS measurements. In other words, both the counter electrode and the reference electrode from the current amplifier and the EIS device are connected with the current collector in the cathode side of the single-cell stack. As schematically sketched on the right part of Fig. 1, the positive electrode (cathode) of the single-cell stack is connected to REF1 + CA2, while the negative electrode (anode) is connected to REF2 + REF3 + CA1. Note that CA1 and CA2 represent, respectively, the current control and measurement through the working and the counter electrodes, and REFs 1, 2 and 3 indicate the control and measurement of the working electrode potential, the reference electrode potential and the counter electrode potential, respectively. Fig. 3 shows schematics and descriptions of various probes (REFs 1, 2, 3 and CAs 1, 2) for EIS measurements, where eight wires equally spaced on both anode and cathode surfaces are used to collect uniformly and effectively the impedance data from the anode-supported single-cell (ASC-3 purchased from H.C. Starck). Using an AC sinusoidal-wave potential perturbation with signal amplitude of 20 mV, the AC impedance of the single-cell stacks can be obtained by measuring the corresponding current response. In the present study, the impedance measurements are carried out at various DC conditions varying from OCV to 0.6 V, each condition covering a range of frequency from 50 mHz to 3 kHz, so that several overlapping responses due to various mechanisms, such as kinetics of electrochemical reactions and diffusions, may be analyzed under different DC loads.

To clearly show how ohmic and polarization resistances are determined from the Nyquist plot, Fig. 4a presents a typical measured impedance spectrum using the design II operated at the OCV condition. In it values of R_Ω and R_P are multiplied by the effective anodic reactive surface area A_{eff} (=16 cm^2) as indicated by RA_Ω and RA_P in Fig. 4a that can be determined from the intersecting points on the real axis of the Nyquist plot. Then the total impedance is the sum of RA_Ω and RA_P. As can be seen, these data points in Fig. 4a can be well represented by a fitting curve derived from an appropriate equivalent circuit model (ECM), as to be discussed in the next subsection. By directly comparing the electrochemical impedance spectra data between these two nearly identical single-cell stacks except using different designs of flow distributors, we should be able to address the question on why the better flow uniformity in interconnects can effectively improve the cell power density.

2.3. Equivalent circuit model

Because the physical and chemical processes of electrochemical devices are usually very complex and non-linear, there is a need

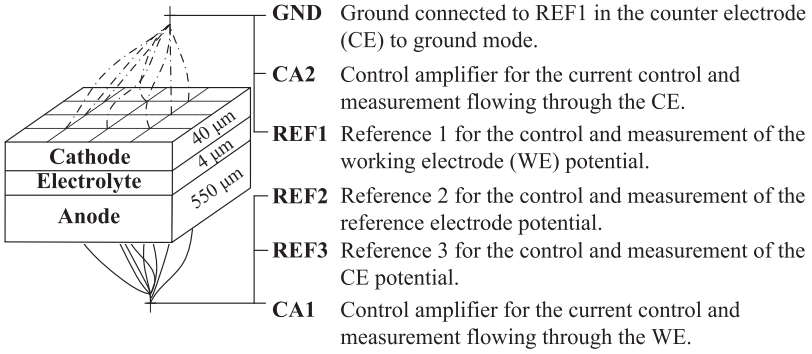

Fig. 3. Schematics of various probes for EIS measurements with detailed descriptions, where eight wires equally spaced on both anode and cathode surfaces are used to collect uniformly and effectively the impedance data from the anode-supported single-cell (ASC-3 purchased from H.C. Starck).

to further develop an appropriate ECM that may be used to fit the experimental impedance data and thus explain some impedance characteristics of the electrochemical devices [11,12]. Fig. 4b shows a typical ECM for the total impedance that often consists of a number of basic lumped elements of the inductors (L), the capacitors (Q), and the resistors (R) in series or in parallel and/or in a combination of both. The corresponding mathematic expression of the total impedance for the present single-cell stacks may be represented by $Z(i\omega) = Z_L + Z_R + Z_{RQ1} + Z_{RQ2} + Z_{RQ3}$, where the induction impedance $Z_L = i\omega L$ is due to the device's electromagnetic induction, the ohmic impedance $Z_R = R_\Omega$ is contributed by ions/electrons transferring in the electrolyte/conductor, and $Z_{RQj} = R_j/[(i\omega)^{nj}R_jQ_j + 1]$ with the subscript $j = 1, 2, 3$ indicating various contributions from such as the electrodes' porosity, non-uniform distribution of reaction rates, and surface roughness and compositions [9,10]. Values of Z_R ($=R_\Omega$) are real in the complex plane that are independent of frequency and can be determined from the intersecting point along the real axis on the Nyquist plot. On the other hand, the frequency-dependent elements, Z_L and $(i\omega)^{-n}Q^{-1} = Z_P$, have only the imaginary contribution and thus their impedance spectra should be parallel to the imaginary axis [5–7]. Note that Z_P is a basic element, also known as the constant-phase element (CPE) which is commonly used in the ECM for fuel cells. For the present single-cell stacks, three CPEs are applied as indicated by CPE_1, CPE_2 and CPE_3 in Fig. 4b, corresponding to three overlapping arcs or semicircles with their centers positioned at the real axis (Fig. 4a). In this work, the proposed ECM, as shown in Fig. 4b, is used in attempt to explain these measured impedance data.

3. Results and discussion

3.1. Power-generating characteristics and anodic re-oxidation observation

Before presenting the AC impedance spectra, we first present the comparison of power generating characteristics between the two sets of nearly identical single-cell stacks except using different flow distributors (designs I and II) as shown in Fig. 5. In it values of the power density for both cases quickly increase from zero to 281 mW cm^{-2} for the design I and/or 322 mW cm^{-2} for the design II, as values of the current density I_d increase from zero to 400 mA cm^{-2} under loaded conditions. There is a 12.5% increase in the value of the power density for the design II using guide vanes as compared to that of the design I without using guide vanes at the same I_d = 400 mA cm^{-2}, indicating an important point that the higher flow uniformity in flow distributors is, the better cell performance is. Due to very high flow rates ($Q_{H_2} = Q_{AIR} = 60$ l h^{-1}) used in the present study, the fuel and air utilization rates are rather small. Note that the fuel and/or utilization rates can be estimated using the ratio of the effective usage of H_2 and/or air flow rates ($Q_{H_2,eff}$ and/or $Q_{AIR,eff}$) for power generation to the total supply of H_2 and/or air flow rates ($Q_{H_2,total}$ and/or $Q_{AIR,total}$). $Q_{H_2,eff} = nI/2F$ (moles s^{-1}) and $Q_{AIR,eff} = nI/4F$ (moles s^{-1}), where n is the cell number, F is the Faraday constant (=96485 C mole^{-1}), and I is the current. In the present study, $n = 1$, $I_{max} = 6.4$ A (or 400 mA cm^{-2} in current density) for both cases in Fig. 5 to avoid the occurrence of the concentration

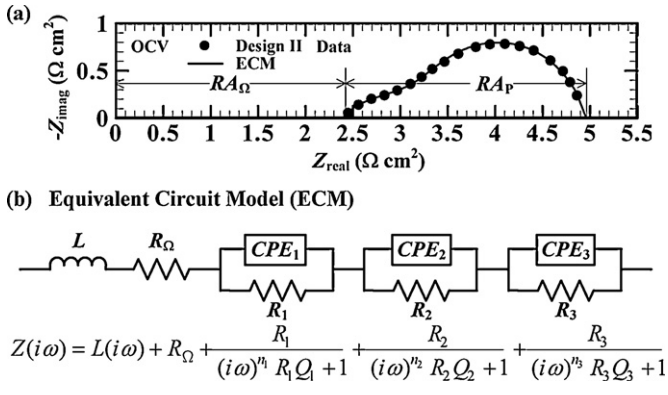

Fig. 4. (a) A typical impedance spectrum obtained at the OCV condition using the design II interconnects with small guide vanes showing the determination of ohmic and polarization impedances (RA_Ω and RA_P). The solid points are the measured impedance data and their fitting line is via the equivalent circuit model as shown in (b) which is used to fit and explain the impedance data of the present single-cell stacks using different designs of flow distributors.

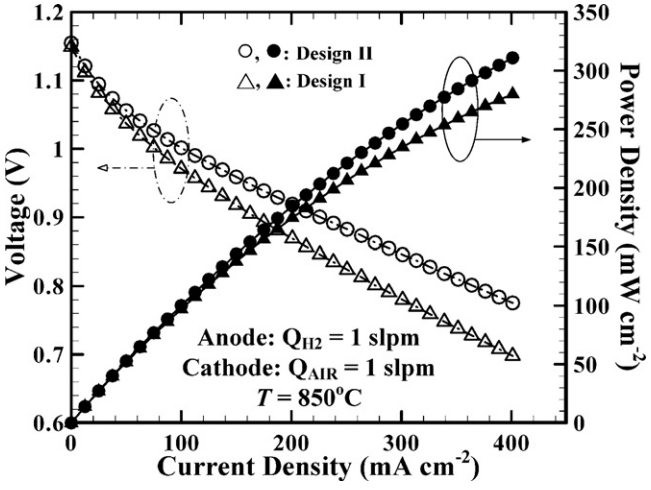

Fig. 5. Comparison of power-generating characteristics between two sets of the single-cell stack under the same experimental conditions except using different designs of flow distributors.

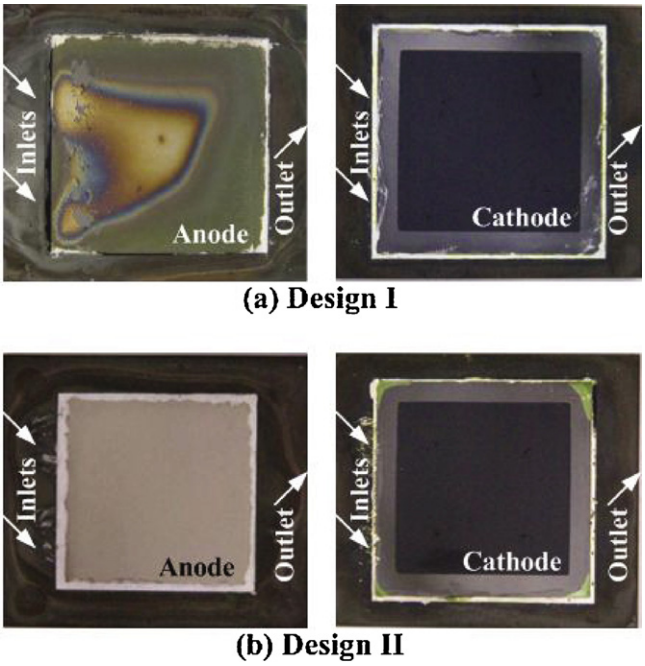

Fig. 6. Photographs of both anode and cathode surfaces of the PEN after 100 h of operation using different designs of flow distributors: (a) Design I and (b) Design II, in which the design I case has severe anodic re-oxidation zones while the design II case using small guide vanes having much better flow uniformity in flow distributors is free from any anodic re-oxidation.

polarization at higher loads, and $Q_{H_2,\text{total}} = Q_{\text{AIR,total}} = 1\,\text{l}\,\text{min}^{-1}$, so that the fuel utilization rate is 4.8% and the air utilization rate is 1.2%.

Fig. 6a and b presents photographs of the anode and the cathode surfaces of the PEN after 100 h of operation for both designs using two different flow distributors, respectively, (a) design I and (b) design II. As can be seen from Fig. 6b, no anodic re-oxidation can be observed in the case of the design II using simple guide vanes having excellent flow uniformity in flow distributors, where the anodic surface still remains a fully reduced metallic Ni/YSZ surface with uniform grey color even after 100 h of the continuous cell operation. On the other hand, under the same experimental conditions, severe anodic re-oxidation zones ($Ni_{1-\delta}O$/YSZ) are observed in the case of design I without using guide vanes having not-so-good flow uniformity in flow distributors, where the anodic catalyst changes colors from green to dark green and/or black with increasing δ (Fig. 6a). Since the same flow rates are carefully applied to both the anode and the cathode ($Q_{H_2} = Q_{\text{AIR}} = 1$ slpm) in the present study to avoid any possible air leakage to the anode, the anodic re-oxidation observed only in the case of design I is thus due to non-uniform flow distributions in interconnects. It is thought that the smaller fuel flow velocities in some of 12 flow rib-channels (design I) can lead to higher fuel utilization. This may further cause a significant drop of the fuel partial pressure (close to zero), the so-called fuel starvation, that can occur locally for some very small fuel flow velocities, eventually resulting in the occurrence of the locally anodic re-oxidation in the case of design I (see Fig. 6a). Note that the anodic re-oxidation can decrease the porosity of the anode which in turn limits the fuel diffusion process and may cause micro cracks at the interface between the anode and the electrolyte. As to the cathode surfaces, both cases (designs I and II) look almost the same even after 100 h of operation (Fig. 6a and b). This is probably because the cathode has much slower reaction rates of oxygen. Hence, these results indicate that the unwanted local re-oxidation of the anode after long time cell operation can be avoided

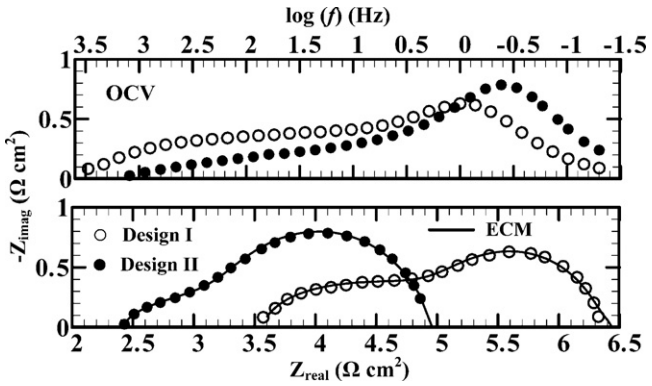

Fig. 7. The Nyquist plot of the two sets of nearly identical single-cell stacks except that the feed headers of the rib-channel flow distributors were different, one with small guide vanes that can significantly increase flow uniformity (design II) and the other without (design I), in which data are measured at the OCV condition over a wide frequency range from 50 mHz to 3 kHz while keeping all operating conditions the same for both cases.

by improving the degree of flow uniformity in flow distributors and thus the longevity of the cell stack may be extended.

It should be noted that the difference of the data between designs I and II (about 12% differences in power density) is not due to the gas-leakage because of the following four reasons. (1) There is no gas-leakage at the frame, because we have carefully applied ceramic sealants on the crofer 22-APU supporting frame for both anode and cathode sides to fix the PEN and to prevent any possible gas leakage at the frame (see Fig. 2b). (2) There is no air leakage to the anode, since we have carefully controlled the flow rate in anode to be at least equal to or higher than that of the cathode. In addition, the present study applies high flow rates ($60\,\text{l}\,\text{h}^{-1}$ and/or 1 slpm controlled by precision flow meters) in both anode and cathode to provide sufficient gases in the single-cell stack and thus make sure no gas-leakage from the outside furnace environment into the cell. (3) With a 3-kg load applied for achieving a good contact of current collectors, the amount of gas-leakage from the cell to the furnace is very small having little influence on the cell performance especially in the high-temperature furnace environment where $T = 850\,^{\circ}\text{C}$. (4) The present results are not obtained from just one-shot experiment, because we have repeated the same experiments for at least three times to confirm the repeatability of these results. Furthermore, the degradation of cell performance is less than 1% after the long time (100 h) operation showing that the PENs have absolutely no cracks at all. Note that the crack of the PENs is the only possible way for the gas-leakage and this does not occur in the present study. Hence, by comparing two sets of nearly identical single-cell stacks under exactly the same experimental conditions except that different designs of flow distributors (designs I and II) are used, we are able to obtain a clear-cut result on the impact of flow distributors to cell performance and impedance spectra when the above arrangements are applied.

3.2. AC impedance spectra at open-circuit voltage and loaded conditions

At the same OCV condition, Fig. 7 presents the comparison of the impedance spectra including both the Bode plot (top) and the Nyquist plot between the two sets of nearly identical single-cell stacks except using different flow distributors (designs I and II), in which the same experimental conditions, e.g., $T = 850\,^{\circ}\text{C}$ and $\dot{Q}_{H_2} = \dot{Q}_{\text{AIR}} = 1000\,\text{ml}\,\text{min}^{-1}$, are applied. These measured impedance data points, as indicated by the circle symbols scanning from ~0 Hz on the right end to the highest frequency (~3 kHz) on the left end in Fig. 7, can be well fitted by the proposed ECM (see Fig. 4b) rep-

Table 1
Comparisons between designs I and II for various key elements in the proposed equivalent circuit model as shown in Fig. 4b.

ECM elements	OCV		1 V		0.8 V		0.6 V	
	I	II	I	II	I	II	I	II
L (μH)	0.494	0.512	0.486	0.504	0.492	0.51	0.496	0.509
R_Ω (Ω)	0.219	0.149	0.221	0.151	0.218	0.150	0.218	0.150
Q_1 (Fs^{n_1-1})	0.019	0.062	0.033	0.105	0.04	0.167	0.048	0.403
n_1	0.855	0.842	0.762	0.79	0.747	0.781	0.736	0.739
R_1 (Ω)	0.031	0.012	0.039	0.01	0.033	0.006	0.032	0.004
Q_2 (Fs^{n_2-1})	0.632	1.46	0.635	1.782	0.713	1.731	0.84	1.788
n_2	0.601	0.605	0.643	0.625	0.645	0.643	0.652	0.634
R_2 (Ω)	0.092	0.053	0.064	0.036	0.054	0.023	0.049	0.021
Q_3 (Fs^{n_3-1})	3.645	4.449	3.664	6.033	5.395	9.331	9.797	12.92
n_3	1	0.931	0.954	0.997	0.946	0.911	0.988	0.918
R_3 (Ω)	0.059	0.099	0.045	0.04	0.021	0.019	0.01	0.01

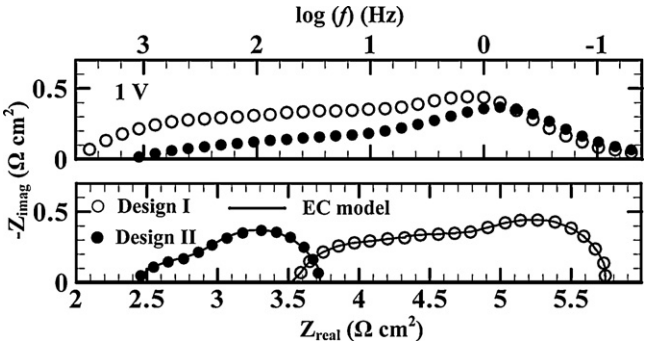

Fig. 8. Same as Fig. 7, but data are measured at the loaded condition when the single-cell stacks are operated at 1 V.

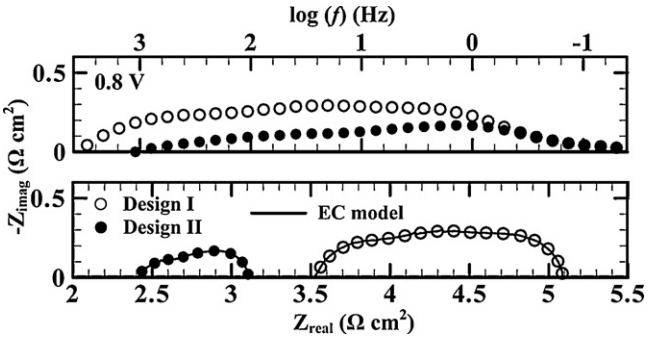

Fig. 9. Same as Fig. 7, but data are measured at 0.8 V.

resented by the solid line on the Nyquist plot. As mentioned in the previous section, the present ECM includes three CPEi (i = 1, 2, 3) corresponding to three overlapping arcs or semicircles, each CPE representing a physical or chemical process. Note that there are

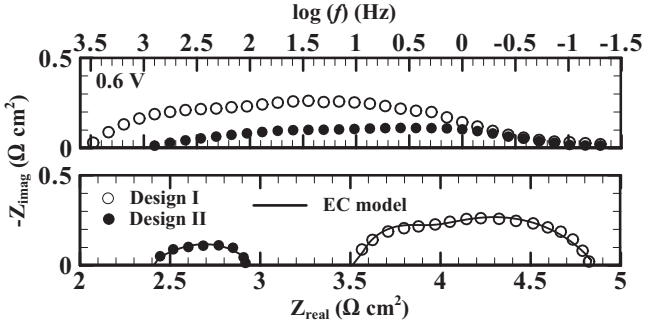

Fig. 10. Same as Fig. 7, but data are measured at 0.6 V.

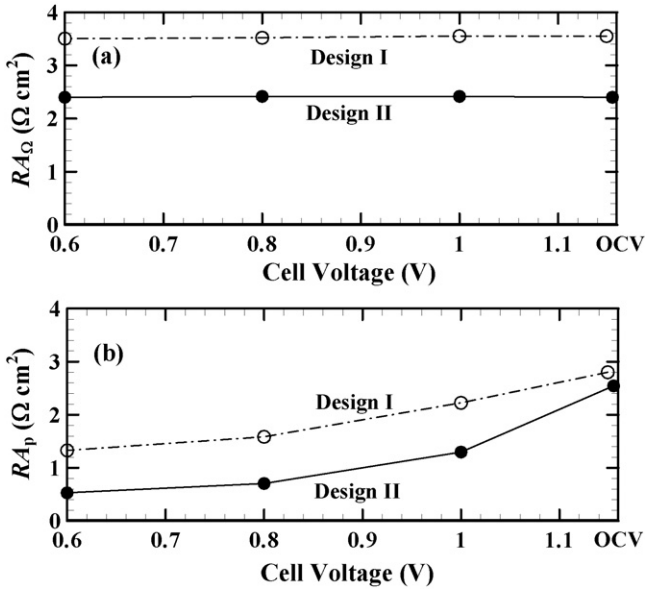

Fig. 11. (a) Comparison of the ohmic resistance between the two sets of nearly identical single-cell stacks using different designs of flow distributors (designs I and II) plotted against different cell voltages varying from OCV to 0.6 V. (b) Same as (a), but for the polarization resistance data.

two intersecting points by the proposed model line on the Z_{real} axis of the Nyquist plot, at which the two corresponding values of Z_{real} are used to determine values of RA_Ω and RA_P (see also Fig. 4a). It is found that $RA_\Omega \approx 3.50\,\Omega\,cm^2$ and $RA_P \approx 2.80\,\Omega\,cm^2$ for the design I without using guide vanes having a total impedance value of $RA_{tot} = RA_\Omega + RA_P \approx 6.30\,\Omega\,cm^2$, while smaller values of $RA_\Omega \approx 2.40\,\Omega\,cm^2$ and $RA_P \approx 2.54\,\Omega\,cm^2$ are found for the design II using guide vanes with $RA_{tot} \approx 4.94\,\Omega\,cm^2$ which is 22% lower than that of the design I (see also Table 1). At the OCV condition, the design I case without using guide vanes having not-so-good flow uniformity in interconnects suffers a larger value of RA_Ω which is 32% higher than that of the design II case. Clearly, this is because the latter case uses simple guide vanes equally spaced around the feed header of rib-channel flow distributors, so that an excellent flow uniformity in flow distributors can be achieved and thus a lower value of impedance is found. As to the polarization resistance, a more modest influence of flow uniformity is found at the OCV condition, where the value of RA_P for the design I case is only 9% higher than that of the design II case. These results measured at the OCV condition seem to be consistent with previous results [16] in which the value of RA_Ω was found to be more sensitive to the effect of redox than the value of RA_P. Therefore, the improvement of flow uniformity in flow distributors is useful to decrease both values of RA_Ω and RA_P of single-cell stacks, in

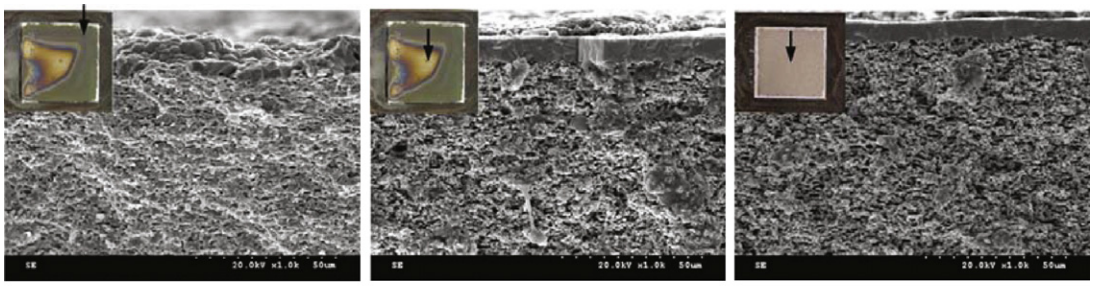

Fig. 12. Comparisons of SEM images showing different anodic microstructures of the PEN after 100 h of operation when two different designs of flow distributors with different degrees of flow uniformity are used.

particular for the decrease of the ohmic resistance when the OCV condition is considered.

Same as Fig. 7 but measured at loaded conditions, Figs. 8–10 show the comparison of the impedance spectra between designs I and II at 1 V, 0.8 V and 0.6 V, respectively. It is found that values of RA_{Ω} for both cases measured at various loaded conditions remain essentially the same as that measured at the OCV condition. In other words, the ohmic resistance does not vary with the loaded cell voltage. This can be more easily from Fig. 11a, where values of RA_{Ω} for both cases are plotted against the cell voltage. Furthermore, the better flow uniformity in interconnects is, the lower values of RA_{Ω} are. As to values of RA_{P} as a function of the cell voltage, a totally different trend is found. Values of RA_{P} for both designs decrease with decreasing the cell voltage, as can be clearly seen in Fig. 11b. This is because decreasing the cell voltage and/or increasing the loaded current can result in more active electrochemical reactions and thus reduce values of RA_{P}. In addition, the percentage differences in values of RA_{P} between designs I and II, defined as $(RA_{P,I} - RA_{P,II})/RA_{P,I}$, increase as the cell voltage decreases, which are, respectively, from 9% at OCV to 42% at 1 V, 56% at 0.8 V and 60% at 0.6 V (see Fig. 11b). The higher values of RA_{P} found in the design I case as compared to that of the design II case are again attributed to the locally anodic re-oxidation occurring only in the design I case. As pointed out by Pihlatie et al. [22], the anodic porosity can be significantly decreased by the oxidation of Ni to NiO due to the volume increase of NiO which is 69% more in volume than Ni. Consequently, for the design I case, the diffusion processes of hydrogen fuel and steam in anode are depressed, resulting in a decrease of available three-phase boundary length and thus an increase in values of RA_{P}.

Concerning the Bode plots on the top of Figs. 7–10, it provides the frequency information of the present impedance data including three summit frequencies (f_{summit}) that correspond to the last three terms (Z_{RQ1}, Z_{RQ2}, Z_{RQ3}) or three overlapping arcs in the proposed ECM (see Fig. 4b and Table 1) as also plotted in the Nyquist plot. Each of them may reflect a physical or chemical process with reference to Laurencin et al. [16]. For Z_{RQ1} at the high frequency range in the model (Fig. 4b), $f_{summit,1}$ = 954–1139 Hz (design I) and 827–1101 Hz (design II) that may be related to anodic chemical reaction processes [16]. For Z_{RQ2} at the middle frequency range, $f_{summit,2}$ = 18–25 Hz (design I) and 11–28 Hz (design II) that may be dominated by gas diffusion processes near the electrode structure [16]. For Z_{RQ3} at the low frequency range, $f_{summit,3}$ = 0.7–1.7 Hz (design I) and 0.4–1.5 Hz (design II) that may be influenced by electrochemical reaction processes in the cathode [16]. However, it is far beyond the scope of the present study to identify actually how many physically relevant processes the impedance of the single-cell stack includes. This is because the impedance of the single-cell stack is very complex that may involve many physical and chemical processes. Therefore, these three overlapping arcs ($Z_{RQ1} + Z_{RQ2} + Z_{RQ3}$) corresponding to three summit frequencies reflecting different physical processes in the proposed model (Fig. 4b) should be viewed with some caution due to the limited numbers of impedance experiments conducted. Nevertheless, the present impedance data and their associated discussion do provide a clear-cut result based on values of RA_{Ω} and RA_{P} that can be used to explain why by improving flow uniformity in interconnects can effectively reduce the impedance and thus increase the cell performance of the single-cell stack.

3.3. Anodic microstructure analysis by SEM

Fig. 12 presents comparisons of SEM images showing three different anodic microstructures of the PEN when using two different designs of flow distributors (designs I and II), respectively, (a) the design I case taken from the anodic re-oxidation zone (NiO), (b) the design I case taken from the still Ni catalyst region, and (c) the design II case without the occurrence of re-oxidation (Ni). Note that the annexes on the top left of these SEM images with the arrows show the locations where the samples are taken from. It can be directly seen from Fig. 12a that the occurrence of the unwanted re-oxidation zone on the anodic surface can significantly reduce the porosity of the anode. This in turn depresses the fuel diffusion process through the porous anode possibly making micro cracks at the interface between the anode and the electrolyte and eventually causing the sever degradation of the anodic catalyst. In addition, when the local re-oxidation of the anode occurs, the corresponding location of the Ni-mesh is also oxidized, further inhibiting the pass way of the electrons from the anode to the current collector and thus resulting in an increase of the impedance. On the other hand, when the design II with a very high degree of flow uniformity in flow distributors is applied, the anodic Ni catalyst can be free from the re-oxidation (Fig. 12c). Hence, the improvement of flow uniformity in flow distributors not only can avoid the unwanted local re-oxidation of the anode but also can reduce the impedance, showing the important impact of flow distributors on the performance and the longevity of the cell stack.

4. Conclusions

A clear-cut result concerning the impact of flow distributors on the electrochemical impedance of single-cell stacks is presented. This is achieved by comparing the impedance spectra between two sets of nearly identical single-cell stacks measured by the electrochemical impedance spectroscopy under the open-circuit voltage and at various loaded conditions, where all experimental procedures and conditions are kept the same except using different flow distributors (designs I and II) in these two stacks. Results show that the ohmic resistance for both designs is independent of the cell voltage where values of RA_{Ω} at various loaded conditions are essen-

tially the same as that obtained at the OCV condition, while the polarization resistance is sensitive to the cell voltage where values of RA_P decrease with decreasing the cell voltage (Fig. 11). The latter is because increasing the loaded current and/or decreasing the cell voltage can result in more active electrochemical reactions. As to the impact of flow distributors, the better flow uniformity in flow distributor is, the lower values of RA_Ω and RA_P are. When compared at the same operating conditions (0.6 V at 850 °C), it is found that both values of ohmic and polarization resistances of the single-cell stack using guide vanes having excellent flow uniformity in interconnects are, respectively, 32% and 60% smaller than that without using guide vanes having not-so-good flow uniformity in interconnects. These results explain why the power density of the present single-cell stack can be increased more than 10% by just improving flow uniformity in interconnects (Fig. 5). Moreover, the higher values of RA_Ω and RA_P found in the design I case as compared to that of the design II case are attributed to the locally anodic re-oxidation occurring only in the design I case due to non-uniform flow distributions in interconnects, as also confirmed by SEM microstructure observations (Fig. 12). It is thus concluded that the improvement of flow uniformity in flow distributors not only can reduce the impedance of the cell stack but also can avoid the unwanted local re-oxidation of the anode. As such, the present measurements are useful for further improving the performance and the longevity of planar SOFCs.

As a final remark, we are currently conducting high-pressure experiments in a newly established double-chamber SOFC testing facility. Power generating characteristics and impedance spectra for single-cell stacks using different designs of flow distributors at elevated pressures up to 5 atm will be measured, aiming to provide the basic knowledge for the future development of the high-efficiency SOFC and gas turbine integrating power generation technology. These results will be published in the near future.

Acknowledgments

The authors would like to thank the referees for their valuable comments. This work was continuously supported by the Institute of Nuclear Energy Research (972001INER036, 982001INER040, and 992001INER048) and the National Science Council (NSC97-2212-E-008-085-MY3, 98-2221-E-008-058-MY3, and 98-3114-E-008-004) in Taiwan.

References

[1] C.M. Huang, S.S. Shy, C.H. Lee, J. Power Sources 183 (2008) 205–213.
[2] C.M. Huang, S.S. Shy, H.H. Li, C.H. Lee, J. Power Sources 195 (2010) 6280–6286.
[3] H. Yakabe, Y. Baba, T. Sakurai, M. Satoh, I. Hirosawa, Y. Yoda, J. Power Sources 131 (2004) 278–284.
[4] H. Yoshida, H. Yakabe, K. Ogasawara, T. Sakurai, J. Power Sources 157 (2006) 775–781.
[5] J.R. Macdonald, J. Appl. Phys. 58 (1985) 1971–1978.
[6] J.R. Macdonald, J. Appl. Phys. 61 (1987) 700–713.
[7] J.R. Macdonald, J. Appl. Phys. 65 (1989) 4845–4853.
[8] C.A. Schiller, W. Strunz, Electrochim. Acta 46 (2001) 3619–3625.
[9] C.H. Kim, S.L. Pyun, J.H. Kim, Electrochim. Acta 48 (2003) 3455–3463.
[10] J.B. Jorcin, M.E. Orazem, N. Pébére, B. Tribollet, Electrochim. Acta 51 (2006) 1473–1479.
[11] E. Barsoukov, J.R. Macdonald, Impedance Spectroscopy Theory, Experiment, and Applications, 2nd ed., John Wiley & Sons, Inc., New Jersey, 2005.
[12] Q.A. Huang, R. Hui, B. Wang, J. Zhang, Electrochim. Acta 52 (2007) 8144–8164.
[13] M. Gong, X. Liu, J. Trembly, G. Johnson, J. Power Sources 168 (2007) 289–298.
[14] B. Iwanschitz, J. Sfeir, A. Mai, M. Schütze, J. Electrochem. Soc. 157 (2) (2010) B269–B278.
[15] B. Liu, Y. Zhang, B. Tu, Y. Dong, M. Cheng, J. Power Sources 165 (2007) 114–119.
[16] J. Laurencin, G. Delette, B. Morel, F. Lefebvre-Joud, M. Dupeux, J. Power Sources 192 (2009) 344–352.
[17] K. Hilpert, D. Das, M. Miller, D.H. Peck, R. Weiβ, J. Electrochem. Soc. 143 (1996) 3642–3647.
[18] H.C. Liu, C.H. Lee, Y.H. Shiu, R.Y. Lee, W.M. Yan, J. Power Sources 167 (2007) 406–412.
[19] H. Tu, U. Stimming, J. Power Sources 127 (2004) 284–293.
[20] V.A.C. Haanappel, M.J. Smith, J. Power Sources 171 (2007) 169–178.
[21] V.A.C. Haanappel, A. Mai, J. Mertens, Solid State Ionics 177 (2006) 2033–2037.
[22] M. Pihlatie, A. Kaiser, M. Mogensen, Solid State Ionics 180 (2009) 1100–1112.